INTEGRATION OF A GaN HEMT SOLID-STATE DRIVER AMPLIFIER FOR THE 10 MHz RF SYSTEM OF THE CERN PS

M. Taquet*, G. Gnemmi†, H. Damerau, S. Energico, M. Morvillo, S.Ramberger
CERN, Geneva, Switzerland

Abstract

The progressive obsolescence and the discontinuation of vacuum tube production are driving the transition towards solid-state alternatives in RF acceleration systems. In the 10 MHz RF system of the Proton Synchrotron (PS) at CERN, the discontinuation of a specific tetrode model used in the amplifier chain has motivated the evaluation of solid-state technology as a potential replacement. In particular, amplifiers based on Gallium Nitride High Electron Mobility Transistors (GaN HEMTs) are being considered due to their inherent radiation tolerance. For this purpose, a prototype driver amplifier based on the GaN technology has been built. This contribution presents the different development steps of this prototype, as well as its integration into the 10 MHz RF system. This includes a system-level description of the RF system and of the constraints associated to the integration of such a prototype, followed by its hardware description and qualification process. This qualification was carried out in two steps: firstly through RF measurements without beam, and secondly with a characterization of the system with high-intensity proton beams, under normal operating conditions.

THE 10 MHz RF SYSTEM IN THE PS

The Proton Synchrotron (PS) at CERN accelerates high-intensity protons up to an energy of 26 GeV. The longitudinal beam structure and energy is obtained through the cumulative action of several RF systems [1]. Among those, the main RF system can operate at multiple harmonics of the revolution frequency. It consists of 11 cavities distributed over the entire PS circumference. Each cavity comprises two $\lambda/4$ resonators loaded with ferrite rings. A bias field in these ferrite rings allows tuning of the cavity from 2.8 MHz to 10 MHz [2]. The accelerating field develops across capacitive gaps.

The amplifier chain feeding the power to the cavity relies on tetrode amplifiers. It is composed of a driver stage with three YL1056 tubes and a final stage based on a single RS1084CJ tetrode. While this technology has historically provided robust performance in the high-radiation environment of the PS, it now faces progressive phase-out of key components. The discontinuation of the YL1056 tetrode in 2022 highlights a broader trend of obsolescence in RF vacuum tube technology, raising concerns regarding the long-term availability and maintainability of vacuum tube-based RF systems at CERN. Consequently, alternative solutions, such as the solid-state technology, must be investigated to ensure continued operation.

While Metal–Oxide–Semiconductor Field-Effect Transistors (MOSFETs) are already used in low-radiation areas at CERN [3], higher radiation levels in the 10 MHz cavity locations limit their application. A promising alternative is the Gallium Nitride High Electron Mobility Transistor (GaN HEMT), which offers significantly higher radiation resistance [4,5]. Multiple irradiation campaigns are ongoing to assess the suitability of GaN devices in the PS environment [6–8].

This paper is focused on the integration of an internally developed GaN-based amplifier in the 10 MHz RF system, with the objective of demonstrating the feasibility of replacing the tetrode-based driver stage with a solid-state alternative. For this purpose, an overview of the RF system and the constraints associated with integrating such a prototype amplifier into the existing RF system is first provided. The two main stages of its qualification within the amplifier chain are then discussed: RF measurements without beam, followed by a characterization of the system with high-intensity proton beams, under operational conditions.

THE SOLID-STATE DRIVER

The integration of a solid-state driver amplifier into the existing 10 MHz RF system imposes constraints beyond those associated with driving the final stage to achieve 10 kV at the cavity gaps. These constraints have guided the hardware choices for the amplifier design. As illustrated in the block diagram with the new driver amplifier (Fig. 1), the RF system comprises several feedback control loops designed to reduce beam loading.

A wideband feedback loop around the driver and final amplifiers, as well as the cavity reduces the beam-induced voltage. As the system operates across a large bandwidth over which the phase changes significantly, a tunable element is required to maintain negative feedback in the entire frequency range. This is achieved by means of a tunable grid resonator, installed between the driver and final stages. As a result, the driver amplifier must maintain stable operation over the frequency range while driving a varying load. The grid resonator contributes mainly to the overall group delay of the wideband feedback loop [2], which must be minimized to maximize the achievable stable gain. To mitigate this effect without reducing the real part of the resonator impedance, thereby avoiding an increase in the power required to the driver amplifier, the latter is equipped with a local feedback loop based on the same principle as

* mathieu.florent.taquet@cern.ch
† giulia.gnemmi@cern.ch

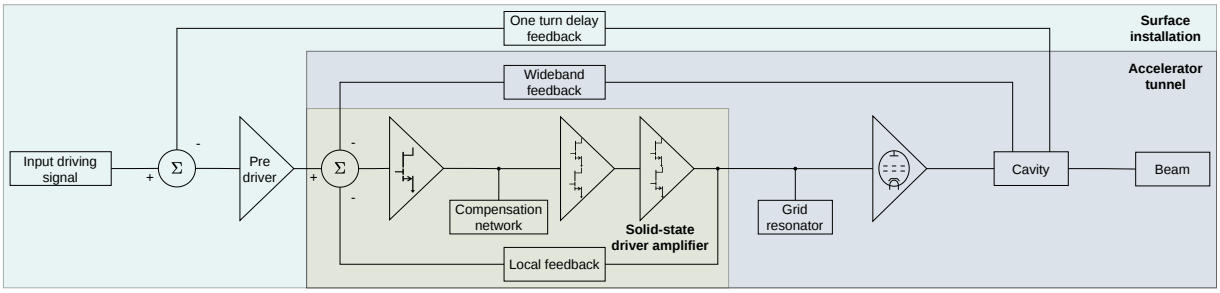

Figure 1: Block diagram of the solid-state driver, integrated in the 10 MHz RF system.

the wideband feedback. The longitudinal beam coupling impedance is further reduced by a digital One Turn Delay Feedback (OTFB) [9]. Since this feedback acts only at the revolution frequency harmonics of the beam and over a narrow bandwidth, it provides gain beyond the stability limit of the wideband feedback.

The combined action of these three feedback loops significantly reduces the longitudinal impedance. Consequently, the driver amplifier must supply additional power, beyond that required to generate 10 kV per cavity gap, to compensate for beam loading. Measurements performed with the previous driver amplifier indicate that its maximum output voltage is 250 V close to the upper frequency limit of 10 MHz.

Taking these constraints into account, a GaN-based prototype driver amplifier has been developed. It consists of three stages. The input buffer provides the summation between its three different input signals (see Fig. 1). It is implemented using a Qorvo QPD1013 device operating in class A. The second stage is composed of two Qorvo QPD1016 devices in a push–pull configuration. It also operates in class A. These two stages enable driving the last stage of the driver amplifier with minimal harmonic distortion, thereby reducing its power consumption. This last stage is based on a dual-chip Macom MAPC-A1511 device in a push–pull configuration, operating in class AB. It is connected to the grid resonator through a transmission-line transformer. It provides the voltage step-up ratio needed to achieve the maximum voltage amplitude at the output while maintaining an acceptable drain voltage swing. To mitigate the phase shift introduced by the amplifier over the range, from 2.8 to 10 MHz, the compensation provided by the grid resonator is insufficient. Although the grid resonator can be de-tuned beyond resonance to increase the phase recovery, this approach should be limited to prevent an increased power demand from the driver amplifier. Therefore, an additional compensation network is present in between the first and second stage of the driver amplifier (Fig. 1). This network is designed to provide a phase lead with increasing frequency, at the expense of a reduced open-loop gain over the frequency range of interest.

The prototype driver amplifier was installed in one of the 10 MHz cavities for qualification tests. RF measurements without beam were performed, followed by a characterization of the system, with beam, under operational conditions.

RF MEASUREMENTS

The first step in characterizing the RF power amplifier stages, i.e. the driver and final stages, in the accelerator tunnel was performed without beam. The amplifier performance was assessed through small-signal measurements using a vector network analyzer. These measurements consist in evaluating the transfer function between the amplifier input and the cavity gap. This characterization is performed both with and without the wideband feedback loop, in frequency steps of 0.5 MHz across the relevant operational bandwidth. This approach serves two main purposes. Firstly, it quantifies the wideband feedback loop gain at each frequency. Secondly, it enables adjustment of the grid resonator at each frequency to achieve the required phase advance, indicated by a symmetric closed-loop response.

The prototype amplifier was installed in the spare cavity of the 10 MHz RF system, referred to as C10-11. It was qualified in C10-11 with the procedure just described. For illustration, the results obtained with the solid-state driver are shown in Fig. 2 at 3 MHz (left) and 10 MHz (right). The prototype exhibited a symmetric closed-loop response. The gain was approximately 24 dB at 3 MHz and 23 dB at 10 MHz, comparable to the existing amplifier. The maximum stable gain was the lowest at 10 MHz, since the group delay was the largest.

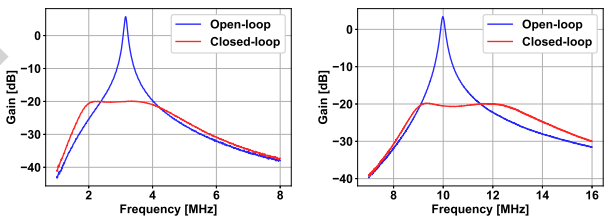

Figure 2: Measurement of the open-loop (blue) and closed-loop gain (red) of the RF system with the cavity tuned at 3 MHz (left) and at 10 MHz (right).

FIRST RESULTS WITH BEAM

As mentioned previously, the driver amplifier must deliver additional power with beam to counteract the beam-induced voltage. The most critical step in the amplifier qualification is therefore testing with the highest-intensity beams.

The properly tuned amplifier was tested with all relevant acceleration cycles, including beams to the neutron Time-of-Flight (n_TOF) facility, the Super Proton Synchrotron (SPS)

north area, the Antiproton Decelerator (AD), and the Large Hadron Collider (LHC). First, these tests were performed without beam to verify that the amplifier behaved as expected in the entire frequency range, especially at critical points of the cycle, such as transition crossing. Subsequently, the beam intensity was gradually increased in order to carefully raise the power delivered by the amplifier. Finally, high-intensity beams were tested with the OTFB.

For illustration, the results of these tests are shown for the beam to AD and for the 72-bunch beam for the LHC. These cases are the most demanding, as they correspond to the highest beam intensities and require to deliver power over a wider frequency range than for other beams.

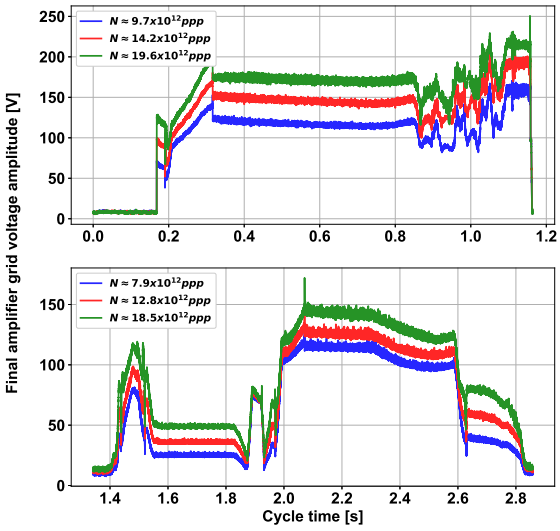

Figure 3: The driver amplifier output voltage amplitude depends on the beam type and intensity. For the beam going to AD, the intensity was swept from an intensity of $N \approx 9.7 \times 10^{12}$ ppp (top, blue) to $N \approx 2 \times 10^{13}$ ppp (top, green). For the LHC-type beam, the intensity was ramped up from $N \approx 7.9 \times 10^{12}$ ppp (bottom, blue) to $N \approx 1.85 \times 10^{13}$ ppp (bottom, green). For completeness, the voltage obtained on intermediate intensities are reported with the red curves. The maximum voltage is obtained with the AD beam, due to transient beam loading. All curves are shown over the relevant cycle period, during which the cavity is pulsing.

A first test was performed by measuring the variation of the amplitude of the driver output voltage, which corresponds to the final amplifier grid voltage, across these two cycles. In Fig. 3, the results obtained for the LHC and AD beams are reported. The LHC 72-bunch beam was successfully accelerated up to the intensity required for the High-Luminosity LHC (HL-LHC) (Fig. 3, bottom) [10, 11]. For the AD beam, the intensity was ramped up to reach the operational intensity of $N \approx 2 \times 10^{13}$ ppp (Fig. 3, top). The final amplifier grid voltage at this intensity, shown by the green curve was a key achievement for the amplifier, as the voltage amplitude reached 250 V, as predicted, and demonstrated that the amplifier was able to deliver the required power.

The performance of the OTFB was then assessed on AD and LHC beams at the operational intensity. This was achieved by measuring the cavity voltage with and without the OTFB at the point in the cycle where the RF power demand is maximum. The measurements on the AD beam shown in Fig. 4 (left) demonstrated that the OTFB was capable of damping the transient beam loading by approximately 12 dB at the first revolution frequency harmonics around the RF frequency, in agreement with its specifications. The performance on the LHC beam was slightly lower, with a damping of approximately 8 dB around the RF frequency. This was a consequence of the lower gain margin of the wideband feedback loop when the cavity is tuned at its maximum frequency.

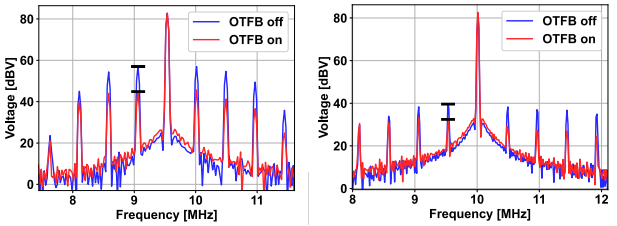

Figure 4: Measurement of the cavity voltage spectrum with (red) and without (blue) the OTFB on the AD beam (left) and on the LHC beam (right). The voltage is damped at the revolution frequency harmonics on both beams, as expected from the OTFB. The feedback gain is measured by taking the difference between the levels indicated by the black bars.

These tests revealed an unforeseen issue. The cavity is equipped with two relays to short-circuit both cavity gaps. Effectively, they lower the cavity impedance and increase its resonant frequency to approximately 23 MHz [12]. During their activation, the cavity resonates at an intermediate frequency of approximately 13 MHz. The gain margin of the wideband feedback loop when the cavity resonance was located at this frequency was insufficient. To increase the gain margin, the next prototype should have a lower gain at these higher frequencies.

CONCLUSION

A complete GaN-based RF driver amplifier has been developed in-house and tested with a cavity in the PS ring. RF and beam-based measurements demonstrate operation over the 2.8–10 MHz range, delivering up to 250 V at the upper end of the band and meeting the requirements for all beam types. These results demonstrate the potential of GaN technology to replace vacuum tubes. A new prototype is under development to improve gain margin and reliability. Following full validation, a series production will be launched to equip all PS cavities with solid-state driver stages.

ACKNOWLEDGMENTS

The authors thank B. Wolley, G. Toma, F. Diaz, A. Lasheen and the PS coordination team and operators for their support during RF measurements and beam tests.

REFERENCES

[1] H. Damerau, S. Hancock, A. Lasheen, and D. Perrelet, "RF Manipulations for Special LHC-Type Beams in the CERN PS", in *Proc. IPAC'18*, Vancouver, Canada, Apr.-May 2018, pp. 1971–1974. doi:10.18429/JACoW-IPAC2018-WEPAF063

[2] D. Grier, "The PS 10 MHz cavity and power amplifier", CERN, Geneva, Switzerland, Rep. CERN-PS-RF-Note-2002-073, 2002. https://cds.cern.ch/record/960421

[3] M. Paoluzzi, "Design of the PBS wideband RF system", CERN, Geneva, Switzerland, Rep. CERN-ACC-Note-2013-0030, 2013. https://cds.cern.ch/record/1621662

[4] A. Polyakov *et al.*, "Radiation effects in GaN materials and devices", *J. Mater. Chem. C*, vol. 1, no. 5, pp. 877–887, 2013. doi:10.1039/C2TC00039C

[5] D. Fleetwood *et al.*, "Radiation effects in AlGaN/GaN HEMTs", *IEEE Trans. Nucl. Sci.*, vol. 69, no. 5, pp. 1105–1119, Jan. 2022. doi:10.1109/TNS.2022.3147143

[6] A. Zimmaro *et al.*, "Investigation of radiation effects on GaN HEMTs for particle accelerators", presented at CHARM-RADWG User Meeting 2024, CERN, Geneva, Switzerland, Jan. 2025. https://indico.cern.ch/event/1500025

[7] G. Gnemmi *et al.*, "Qualification of Gallium-Nitride High Electron Mobility Transistors for the 10 MHz Radio-Frequency systems in the CERN Proton Synchrotron", in *Proc. RADECS 2025*, Antwerp, Belgium, Sep. 2025, pp 1–6. doi:10.1109/RADECS66956.2025.11370393

[8] D. Söderström, G. Lerner, and S.Fiore, "Radiation levels in the PS ring, and estimations for Run 4", CERN, Geneva, Switzerland, 2026.

[9] F. Blas and R. Garoby, "Design and operational results of a one-turn-delay feedback for beam loading compensation of the cern ps ferrite cavities", in *Proc. PAC'91*, San Francisco, CA, USA, May 1991, pp. 1398–1401. doi:10.1109/PAC.1991.164647

[10] G. Arduini *et al.*, "Beam parameters at LHC injection", CERN, Geneva, Switzerland, Rep. CERN-ACC-2014-0006, 2014. https://cds.cern.ch/record/1644771

[11] K. Hanke *et al.*, "The LHC Injectors Upgrade (LIU) Project at CERN: Proton Injector Chain", in *Proc. IPAC'17*, Copenhagen, Denmark, May 2017, pp. 3335–3338. doi:10.18429/JACoW-IPAC2017-WEPVA036

[12] G. Favia, "Study of the beam-cavity interaction in the CERN PS 10 MHz cavities and investigation of hardware solutions to reduce beam loading", Ph.D. thesis, Rome U., Feb. 2017.